Journal of The Electrochemical Society

The Electrochemical Society
Advancing solid state & electrochemical science & technology

OPEN ACCESS

High Durability and Electrocatalytic Activity Toward Hydrogen Evolution Reaction with Ultralow Rhodium Loading on Titania

To cite this article: Merve Akbayrak and Ahmet M. Önal 2020 *J. Electrochem. Soc.* **167** 156501

Journal of The Electrochemical Society, 2020 **167** 156501

High Durability and Electrocatalytic Activity Toward Hydrogen Evolution Reaction with Ultralow Rhodium Loading on Titania

Merve Akbayrak and Ahmet M. Önal[z]

Department of Chemistry, Middle East Technical University, 06800 Ankara, Turkey

Herein, we report the synthesis of titania supported Rh(0) nanoparticles (Rh^0/TiO_2) as electrocatalyst for hydrogen evolution reaction (HER) in acidic medium. Rhodium nanoparticles with an average particle size of 2.54 nm are found to be well-dispersed on TiO_2 surface. Rh^0/TiO_2 with very low loading density (3.79 $\mu g\ cm^{-2}$) was attached on the glassy carbon electrode (GCE) by drop-casting method. Electrocatalytic performance of modified GCE was investigated via linear sweep voltammetry (LSV) in 0.5 M aqueous H_2SO_4 solution after 2000 cycle treatment (Rh^0/TiO_2-2000) and it was found that Rh^0/TiO_2-2000 on GCE exhibits superior electrocatalytic activity (TOF: 11.45 s^{-1} at $\eta = 100$ mV, η_0:−28 mV, $\eta_{10\ mA\ cm^{-2}}$: −37 mV, j_0: 0.686 mA cm^{-2} and Tafel slope: 32 Mv dec^{-1}). More importantly, it provides outstanding long-term stability (10000 cycles) at room temperature for HER, which makes Rh^0/TiO_2-2000 a promising electrocatalyst for hydrogen generation.
 [DOI: 10.1149/1945-7111/abb9cf]

Manuscript submitted July 1, 2020; revised manuscript received September 14, 2020. Published October 9, 2020. *This paper is part of the JES Focus Issue on Organic and Inorganic Molecular Electrochemistry.*

Supplementary material for this article is available online

For the last decades, finding clean, renewable, and sustainable energy sources is one of the most important research area.[1] In this regard, scientists focus their attention on the hydrogen mainly because of its i) high abundance; ii) high energy conversion efficiency; and iii) non-toxicity.[2–4] Most of the current hydrogen generation methods such as catalytic steam reforming of natural gas or the light oil fraction with steam at high temperatures are associated with greenhouse effect.[5–7] On the other hand, electrochemical splitting of water with no emission is the cleanest method and plays an important role in the sustainable production of hydrogen. Water splits into hydrogen and oxygen at 1.23 V cell voltage under standard conditions according to the following reaction; $H_2O_{(liq)} \rightarrow H_{2(g)} + ½\ O_{2(g)}$.[8,9] At the cathode compartment hydrogen production occurs by proton reduction ($E^0 = 0$ V vs NHE) and at the anode compartment oxygen production occurs by water oxidation ($E^0 = +1.23$ V vs NHE) in acidic medium.[10]

Platinum (Pt) is the most commonly used catalyst for the hydrogen evolution reaction (HER). However, due to its high cost, low abundance, and low stability, the studies on finding an alternative electrocatalyst to Pt or reducing the amount of Pt in the catalysts are still an area of interest for the scientific community. The Volcano plot is one of the most important guide and metal hydride (M–H) bond strength is one of the most important indicator in designing a new efficient catalyst for water splitting. For the ideal catalyst, M–H bond strength should be kept optimum because it affects both adsorption of the reactants on the catalyst's surface or desorption of the products from the surface of the catalyst.[11] Pt is at the top of the volcano plot and Rhodium (Rh), on the other hand, is the nearest metal to Pt with a very small ΔG value.[12,13] Therefore, the design and synthesis of efficient Rh containing electrocatalysts for HER has been one of the most studied topics in recent years.[14–19] Although the scarcity and the high cost of Rh seem to be disadvantages, it is one of the best alternatives to Pt with superior stability even at a very low metal concentration. To decrease the metal amount, nanosized catalysts with a high surface/volume ratio have been designed.[20] The achievement of highly dispersed metal nanoparticles (MNPs) with small particle size results in a large number of catalytically active sites, which increases the electrocatalytic efficiency. However, there is a strong requirement to use supporting materials such as carbon,[21] graphene,[22] metal-organic frameworks,[23] and metal oxides[24,25] for stabilizing MNPs.[26]

Among the various metal oxides, titanium dioxide (TiO_2) is a widely used supporting material in the catalyst field because of its high availability, low cost, high chemical and thermal stability, and non-corrosive property.[27] TiO_2 with a large surface area ranging from 10 to 300 $m^2\ g^{-1}$ can be used as a support to prevent the aggregation of metal nanoparticles.[28] The choice of supporting material is one of the most important factor that affects the activity of the catalyst. The electronic structure of the supported metal can be drastically tuned by the interactions between the supporting material and the metal which enhances the performance of the catalyst.[29] Zheng et al. used Pt/TiO_2 composites for HER and reported that Pt–O interaction weakens the H adsorption which contributes to the Tafel step and Pt–Ti interaction facilitates the Volmer step by enhancing H_2O adsorption.[30] Rh is very close to Pt in the volcano plot and a similar relationship may also occur for Rh/TiO_2. Moreover, the performance of HER can be enhanced by not only changing the electronic structure of the supported metal, but also using the spillover effect effect of the support. In the hydrogen spillover process, adsorbed hydrogen migrates from one surface to another and hydrogen adsorbing sites could be separated from desorbing sites.[31] Zhu et al. found that strong binding sites of Rh easily adsorb the hydrogen and desorption of hydrogen occurs at relatively weak Si binding sites due to the spillover process.[16] In another study, the spillover process between Rh and titania was monitored via IR spectroscopy and it was reported that molecular H_2 dissociates on Rh nanoparticles and H atoms spillover onto the titania.[32] Spillover effect may also enhance the HER activity of Rh/TiO_2. Furthermore, in our previous work, Ruthenium (Ru) was impregnated on the surface of the titanium(IV), zirconium(IV), and hafnium(IV) oxide supports and Ru supported titania was found to show better electroactivity towards HER as compared to hafnia and zirconia in acidic solution.[24]

In light of these information, we prepared Rh/TiO_2 catalyst to be used for HER in acidic medium.

Since one expects higher activity of Rh as compared to Ru, we decreased both loading of Rh in the catalyst and loading density on the electrode surface.

In this study, the preparation, characterization, and the investigations of electrocatalytic activity of Rh^0/TiO_2-2000 (0.5% wt. Rh) towards hydrogen evolution reaction are presented. After the impregnation and reduction of Rh^{3+} ions on the titania surface, the obtained catalyst was attached to the surface of GCE and the modified electrode was subject 2000 potential cycling between −0.5 and 0.5 V vs Ag/AgCl. The electrochemical properties of the

[z]E-mail: aonal@metu.edu.tr

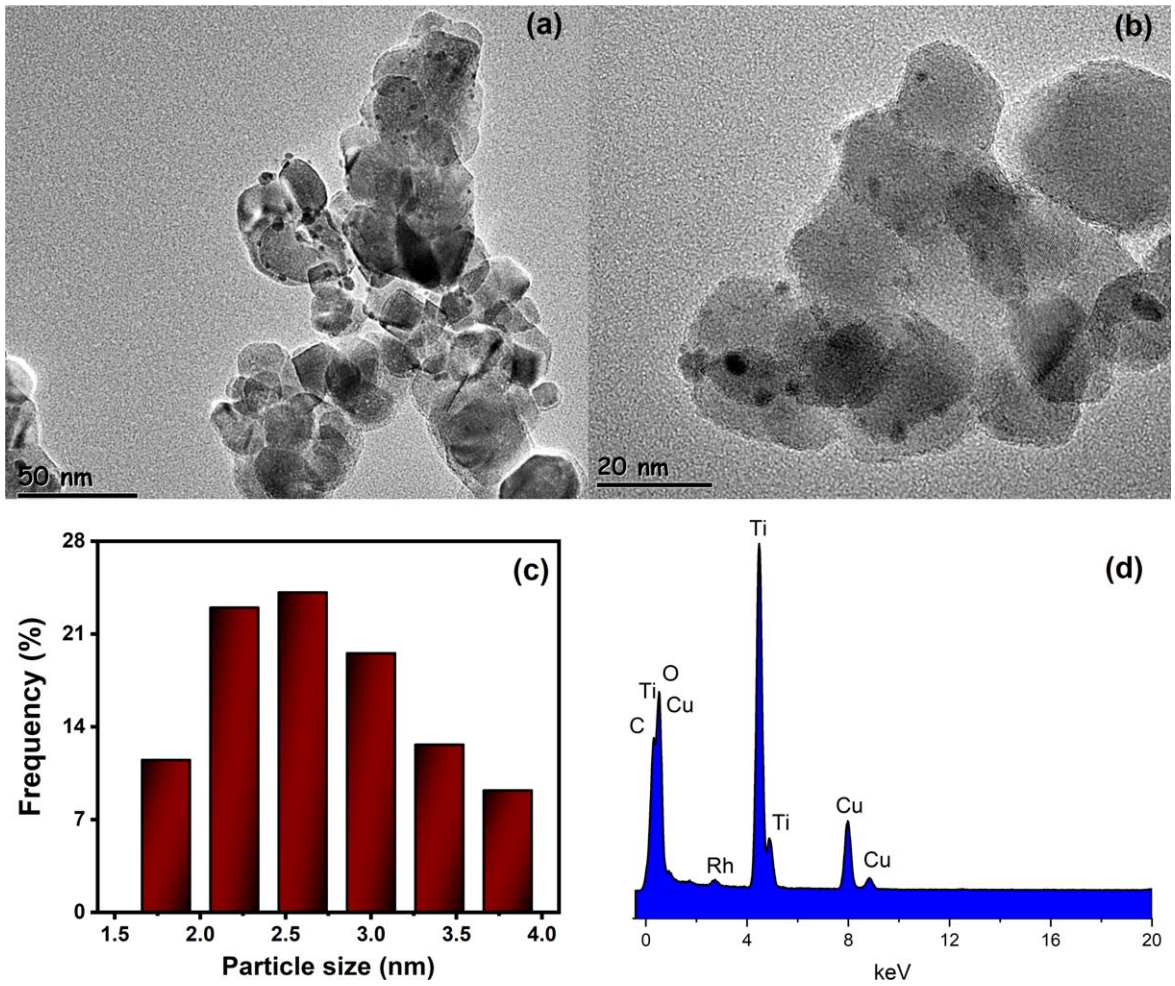

Figure 1. TEM images of Rh^0/TiO_2 (a), (b), the histogram showing the particle size distribution (c), and the corresponding TEM-EDX spectrum (d).

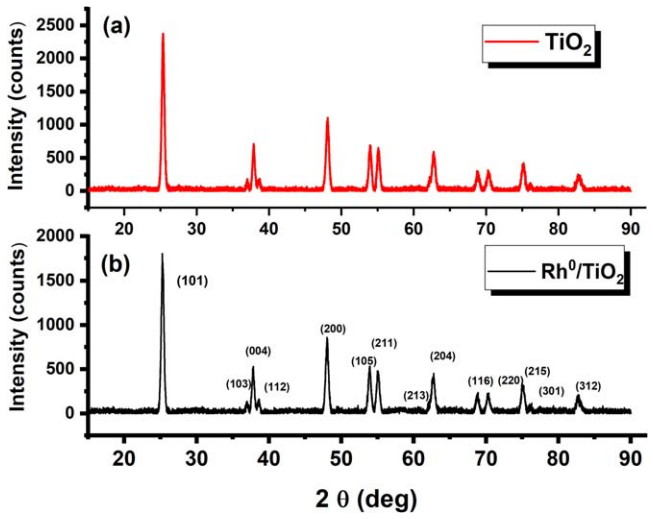

Figure 2. Powder XRD pattern of (a) TiO_2 and (b) Rh^0/TiO_2 (0.50% wt. Rh).

Rh^0/TiO_2 modified GCE electrode, both before (Rh^0/TiO_2) and after (Rh^0/TiO_2-2000) potential cycling, was investigated in acidic environment for HER. Rh^0/TiO_2-2000 was found to be a highly efficient electrocatalyst in 0.5 M H_2SO_4 solution for HER with extremely low mass loading 3.79 μg cm^{-2}, 32 mV dec^{-1} Tafel slope, 37 mV overpotential at j = 10 mA cm^{-2} and 0.686 mA cm^{-2} exchange current density. Moreover, Rh^0/TiO_2-2000 on GCE, maintains its electrochemical activity even after 10000 scans and exhibits outstanding stability for HER in acidic medium at room temperature.

Experimental

Preparation of the catalyst (0.5 wt.% Rh^0/TiO_2).—600 mg of TiO_2 powder and 7.78 mg of $RhCl_3.3H_2O$ salt were stirred together in 100 ml H_2O for 18 h at room temperature. 10 ml of 3.0 mM $NaBH_{4\ (aq)}$ solution was added dropwise to this mixture. After 1 h stirring, Rh(0) nanoparticles were successfully impregnated on TiO_2. After the centrifugation (10 min at 8000 rpm), washing (with 100 ml H_2O), and drying (under vacuum at 60 °C for 12 h) processes, 587 mg of Rh^0/TiO_2 was obtained. According to ICP-OES analysis, the Rh metal content of Rh^0/TiO_2 was determined as 0.50% wt. Rh^0/TiO_2 was also analyzed by TEM, TEM-EDX, XPS and XRD analysis. Note that the materials and characterization section was given in supporting information.

Electrochemical measurements.—For all electrochemical studies, a three-electrode system (modified GCE, Ag/AgCl in 3 M NaCl and Pt wire as a working, reference and counter electrode, respectively) and Gamry PCI4/300 potentiostat–galvanostat were used. Before its modification, the GCE was polished to a mirror finish with alumina polishing suspension. To prepare the catalyst ink, 50 mg of Rh^0/TiO_2 and 400 μl Nafion solution were dispersed in 2 ml isopropanol by sonication for 2 h. 2.5 μl of homogeneous ink was dropped onto cleaned GCE (area = 0.07 cm^2) and dried at RT for 3 h. Note that, for all tests, the Rh amount on GCE kept constant

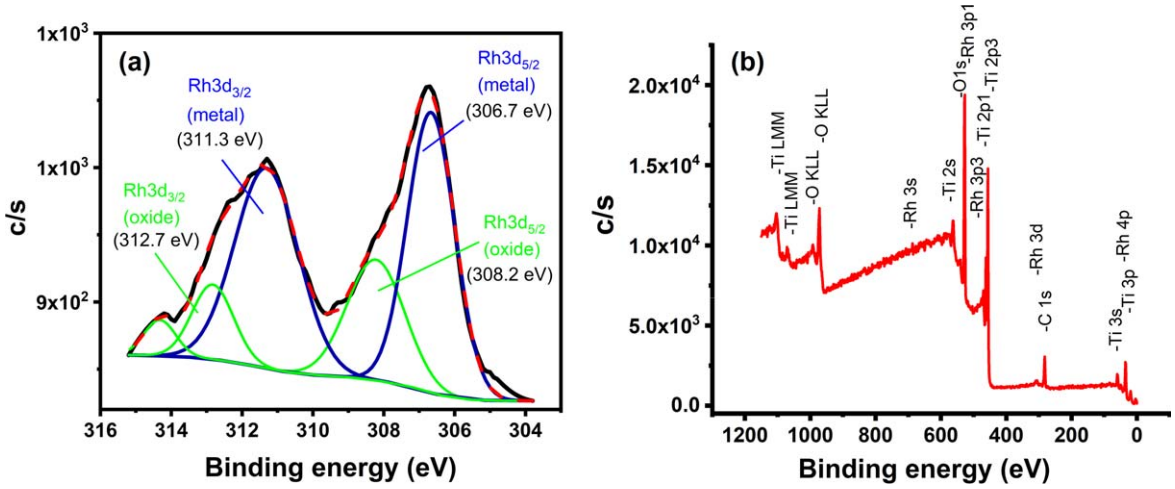

Figure 3. (a) XPS spectrum of Rh 3d bands, (b) The survey-scan XPS spectrum of Rh^0/TiO_2.

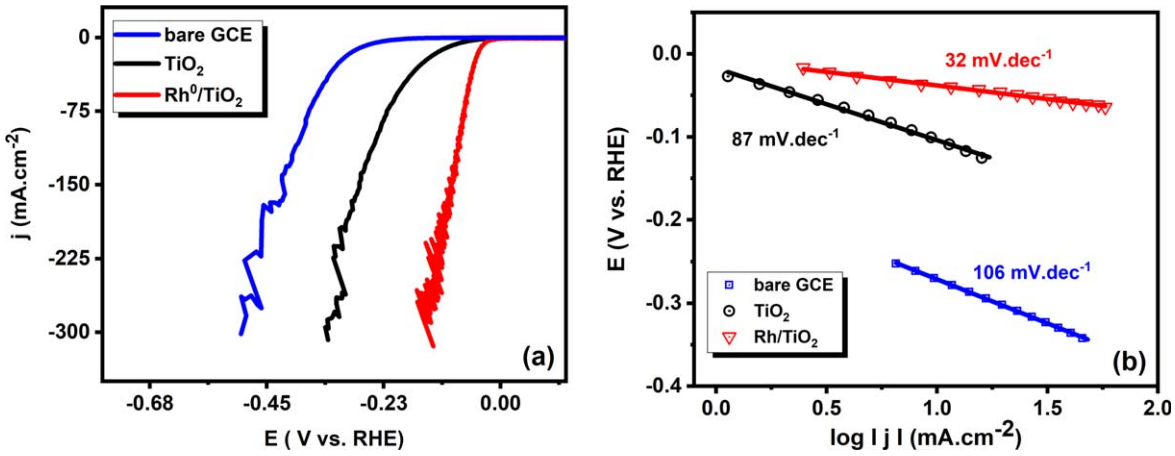

Figure 4. (a) Polarization curves of the treated electrodes (bare GCE, TiO_2 and Rh^0/TiO_2 catalyst on GCE) at 5 mV s^{-1} scan rate in 0.5 M H_2SO_4 and (b) the corresponding Tafel curves.

as 3.79 μg cm^{-2} and for the control tests, Pt/C electrode was prepared by following the same procedure given above.

Linear sweep voltammetry method (LSV) with a 5 mV s^{-1} scan rate in 0.5 M H_2SO_4 solution was used to investigate the electrochemical behavior of catalysts on GCEs. The potentials obtained from polarization curves were reported against reversible hydrogen electrode (RHE) by adding a value of ($E°_{Ag/AgCl}$ + 0.059 pH) V ($E°_{Ag/AgCl}$ = 0.210 V).[33] The electrochemical impedance spectroscopy (EIS) studies were conducted at −13, −23, −33 and −43 mV vs RHE (frequency range: 0.1–100,000 Hz). Note that, before the electrocatalytic test of Rh^0/TiO_2, pretreatment has been performed by applying 2000 cycles between −0.5 and 0.5 V vs Ag/AgCl and the treated electrode was represented as Rh^0/TiO_2-2000. This potential range was also used to test electrocatalytic stability with a voltage scan rate of 50 mV s^{-1}. To investigate the Faradic efficiency, the amount of hydrogen gas produced was determined via Hoffmann apparatus and related calculations are given in the SI part.

Results and Discussion

Titania (TiO_2) supported rhodium NPs (Rh^0/TiO_2) were prepared by impregnation and reduction of Rh^{3+} ions on the TiO_2 surface and characterized by several analytical instruments. TEM analysis was performed to investigate the size of the Rh NPs. As seen in Figs. 1a and 1b, highly dispersed Rh NPs (the mean particle size = 2.54 ± 0.56 nm) were formed on titania (Rh particle size is in the range between 1.8 and 3.8 nm (Fig. 1c)). TEM-EDX given in Fig. 1d confirms the presence of Rh NPs on the surface of TiO_2. However, due to the 0.5% wt. Rh loading, there is no peak belonging to the Rh NPs in the XRD spectra (Fig. 2b). According to the XRD results of TiO_2 and Rh^0/TiO_2, there is no change in the crystal structure of titania after Rh impregnation (Figs. 2a–2b).

The oxidation states of Rh NPs in Rh^0/TiO_2 were investigated with XPS analysis. As seen in Fig. 3a, the peaks which belong to $3d_{5/2}$ and $3d_{3/2}$ bands of metallic rhodium appear at 306.7 eV and 311.3 eV, respectively.[34] On the other hand, the peaks at 308.2 eV and 312.7 eV show the oxides species of rhodium.[35] The survey-scan XPS spectra of Rh^0/TiO_2 given in Fig. 3b provides further evidence for the existence of Rh(0) NPs on TiO_2 nanopowder's surface.

Electrocatalytic activity of Rh^0/TiO_2 modified GCE was investigated by recording polarization curves in 0.5 M H_2SO_4 solution. Since the electrocatalytic activity of the modified electrode was found to be improved gradually after potential cycling between between −0.5 and 0.5 V vs Ag/AgCl, Rh^0/TiO_2 modified GCE was subjected to the potential cycling until no more change was noted in the onset potential. This point was reached after 2000 cycles of CV treatment[36] in 0.5 M H_2SO_4 solution. To check if GCE or TiO_2 without rhodium show any activity in HER, 2.5 μl Rh^0 free aliquot was dropped onto a polished GCE. Bare GCE and TiO_2 modified GCE were used as cathodes in three-electrode systems. The observed improvements in the electrochemical activities of TiO_2, bare GCE and Rh^0/TiO_2 during the treatment (Figs. S2a–S2b, Tables SI, SII is available online at stacks.iop.org/JES/167/156501/mmedia), can be

Table I. Various reported Rh and Pt based HER electrocatalysts in 0.5 M H_2SO_4.

Entry	Catalyst	Loading density (μg cm^{-2})	η_0 vs RHE (mV)	η (mV)	Tafel Slope (mV dec^{-1})	j_0 (mA cm^{-2})	References
1	Rh Nanowires[b)]	—	−140	>−100	23	—	15
2	Rh/Si[a)]	193		83.3@-10	24	0.00858	16
3	Rh-Au-SiNW-2[b)]	255	—	62@-10	24	0.0479	17
4	Rh Hollow Nanoparticles[b)]	2.26	∼−20	28.1@-10	24	—	18
5	PtRu/CC1500[b)]	1.6 (ECSA normalized)	—	8@-10	25	2.44	36
6	Pt-FeNi@C[b)]	85.7		50@-21	26.1		41
7	Rh_2P/NC[a)]	700	0	9@-10	26	2.5	19
8	Rh_2P/C[b)]	3.79	—	5.4@-5	—	—	42
9	*in situ*- Rh/C[b)]	—	∼25	30@-10	28.4	—	14
10	10% Pt/C[b)]	75	−13	26@-10	27	0.54	This work
11	Pt/VG-SPE[b)]	41.92	–	60@-10	27	–	43
12	PtCu/CoP[b)]	3.136	∼0	20@-10	28	—	44
13	Rh_2P[a)]	133	—	14@-10	31.7	—	45
14	**Rh@TiO_2-2000**[b)]	**3.79**	**−28**	**37@-10**	**32**	**0.66**	This work
15	**Rh@TiO_2-2000**[b)] **(after 10000)**	**3.79**	**−29**	**40@-10**	**33.1**	**0.71**	This work
16	0.8%Pt-Naf[b)]	0.2 (ECSA normalized)	—	34@-10	33	5.58	46
17	CS-PdPt[b)]	255	—	26@-10	33	—	47
18	Pt–TiO_2 NS[b)]	16.8	—	35@-10	33	1.01	48
19	Rh-MoS_2[b)]	—	—	67@-10	65	0.1142	49
20	Ni-Pt film[b)]	—	—	90@-10	41	—	50
21	Rh_2S_3[b)]	153		122@-10	44		51
22	$Rh_3Pb_2S_2$/C[b)]	28	—	87.3@10	45.6	—	52
23	Ni_1Rh_1[b)]	169	∼0	64@-10	46	0.692	53
24	Ni@Pd-Pt[b)]	485.9	—	37@-10	47	—	54
25	$MoSe_2$@Rh[b)]	—	—	192@-10	47	—	55
26	Rh–Ag/SiNW-2[a)]	140	—	120@-10	51	0.0871	56
27	Rh Nanoislands[a)]	—	—	—	55	—	57
28	Rh[b)]	169	−19	190@-10	92	0.190	53

a) without and b) with iR compensation.

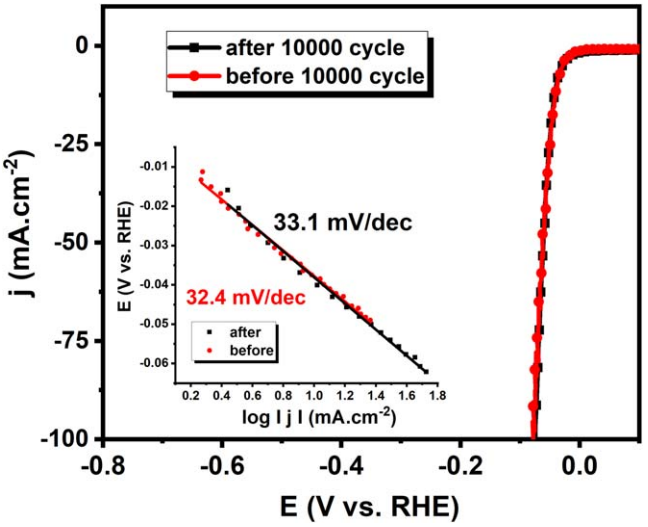

Figure 5. (a) The voltammograms of Rh^0/TiO_2 before and after stability test (10000 CV cycles refers to 55.5 h in 0.5 M H_2SO_4) Inset: Corresponding Tafel plots.

attributed to cathodic deposition of Pt originating from the anodic dissolution of Pt counter electrode.[37–39] The amount of Pt deposited on Rh/TiO_2-GCE after 500, 1000 and 2000 cycles, were determined as 0.52, 6.38 and 17.94 Pt to Rh (mole/mole) ratio, respectively by using ICP-OES. For the bimetallic catalyst, besides metal-support interaction metal-metal interactions are also important in HER. Therefore, the observed improvement in the electrocatalytic activity of Rh/TiO_2-2000 can be attributed not only to Pt deposition but also to Rh-Pt interaction.[40] Note that there is no improvement after 2000 cycles for the Rh^0/TiO_2 (Fig. S2b).

Rh^0/TiO_2-2000 shows superior electrocatalytic activity in 0.5 M H_2SO_4 solution for HER with ultralow mass loading of Rh (3.79 μg cm^{-2}). The polarization curves belonging to bare GCE, TiO_2 and Rh^0/TiO_2-2000 modified GCE after CV treatment (2000 cycle) were presented in Fig. 4a and corresponding Tafel curves were given in Fig. 4b (See SI for the Tafel slope calculation). Tafel slopes of bare GCE, TiO_2 and Rh^0/TiO_2-2000 modified GCE were calculated as 106, 87, and 32 mV dec^{-1}, respectively (Fig. 4b, Table SI). An inspection of Table I reveals that the Tafel slope of Rh^0/TiO_2-2000 is closer to that of commercial 10% Pt/C (27 mV dec^{-1} (Fig. S3)) and comparable to the reported catalysts. Tafel slope is an important parameter to determine the mechanism of HER. The HER mechanism consists of mainly two steps; the first one is the adsorption of H atom to the catalyst surface (Volmer step) and the second one is the desorption of adsorbed hydrogen (H_{ads}) atoms (Heyrovsky or Tafel steps).[9] (See SI for the information on the related mechanism). The calculated Tafel slope (32 mV dec^{-1}) for Rh^0/TiO_2-2000 modified GCE indicates that the HER mechanism fits the Volmer −Tafel mechanism and the rate determining step is the electrochemical desorption of adsorbed hydrogen atoms. The overpotential (η) values at j = 10 mA.cm^2 for Rh^0/TiO_2-2000 and TiO_2 were found as 37 mV and 104 mV vs RHE. The lower η of Rh^0/TiO_2-2000 makes it superior over most of the reported Rh based catalyst such as Rh/Si (entry 2), Rh_2S_3 (entry 21), $Rh_3Pb_2S_2$/C (entry 22), Rh-Ag/SiNW (entry 26), and Rh (entry 28) (Table I).

To investigate the intrinsic activity of Rh^0/TiO_2-2000, the exchange current density (j_0) and TOF values were calculated as described in SI. It is found that Rh^0/TiO_2-2000 provides an exchange current density of 0.686 mA cm^{-2} which is superior as compared to the reported Rh based catalysts listed in Table I. On the other hand, the TOF values calculated by copper underpotential deposition (UPD) method for Rh^0/TiO_2-2000 in 1 M H_2SO_4 are found as 0.80, 1.44, and 11.45 s^{-1} at 20, 50, and 100 mV (vs RHE), respectively (Fig. S1b). Moreover, the TOF value was also calculated from chronopotentiometry. For this purpose, the constant current was applied at an overpotential of 100 mV for 1 h in 0.5 M H_2SO_4 then, the number of moles of H_2 generated was divided to the number of moles of Rh on the electrode surface and the time. According to this calculation, the TOF value was found to be 11.2 s^{-1} at an overpotential of 100 mV which is quite similar to the TOF value calculated from the UPD method (Fig. S1b). It was reported that Pt catalyst exhibits a TOF value of 0.8 s^{-1} at 0 V in HER[58] which is the same as the TOF value obtained for Rh^0/TiO_2 at η = 20 mV.

The durability of Rh^0/TiO_2-2000 was tested by applying 10000 cyclic scans at a scan rate of 50 mV.s^{-1} in the H_2SO_4 solution (0.5 M). The polarization curves which were obtained before and after the stability test (Fig. 5) indicate that there is a negligible change in the onset potential (−29 mV), overpotential at j = 10 mA cm^{-2} (40 mV@-10) and Tafel slope (33.1 mV dec^{-1}). According to these results, one may conclude that Rh^0/TiO_2-2000 is a highly durable electrocatalyst and provides superior stability in HER as compared to the various Rh catalysts in literature such as Rh_2P@NC[19] (1000 cycles), Rh_2P (1000 cycles),[42] Ni_1Rh_1 (2000 cycles).[53] Kim et al. reports that $Rh_3Pb_2S_2$ preserved HER activity even after 10000 scans with a small cathodic shift in the η.[52] However, $Rh_3Pb_2S_2$ requires very harsh preparation techniques and higher mass loading as compared to Rh^0/TiO_2-2000.

Electrochemical impedance spectroscopy (EIS) method was also studied to determine the electrocatalytic activity of Rh^0/TiO_2-2000 at the potential 240, 250, 260, and 270 mV vs Ag/AgCl in 0.5 M H_2SO_4 (Fig. 6a). The observed semicircles at low and high

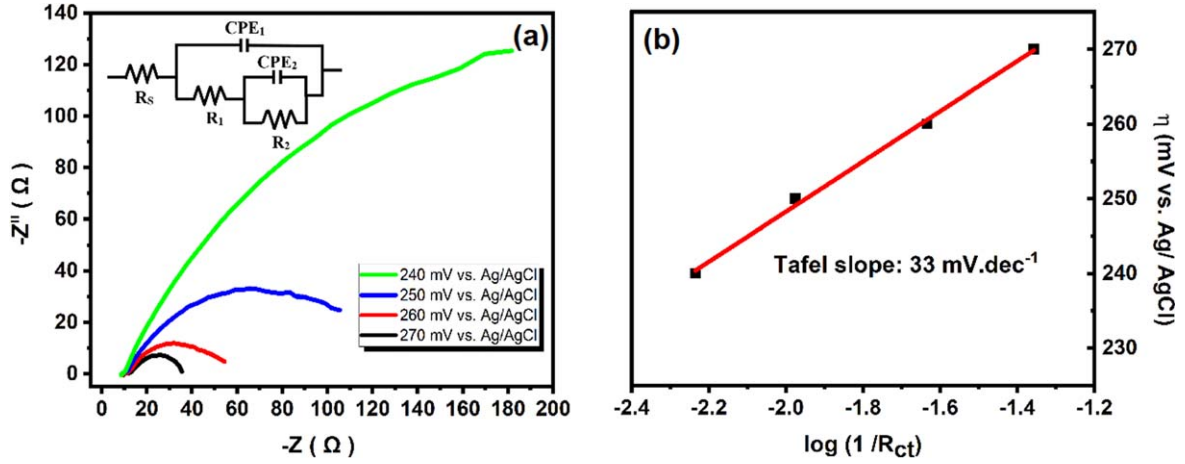

Figure 6. (a) The Nyquist curves of Rh^0/TiO_2 at 240, 250, 260 and 270 mV (vs Ag/AgCl) potentials (b) The Tafel plot of Rh^0/TiO_2 obtained from the impedance measurements.

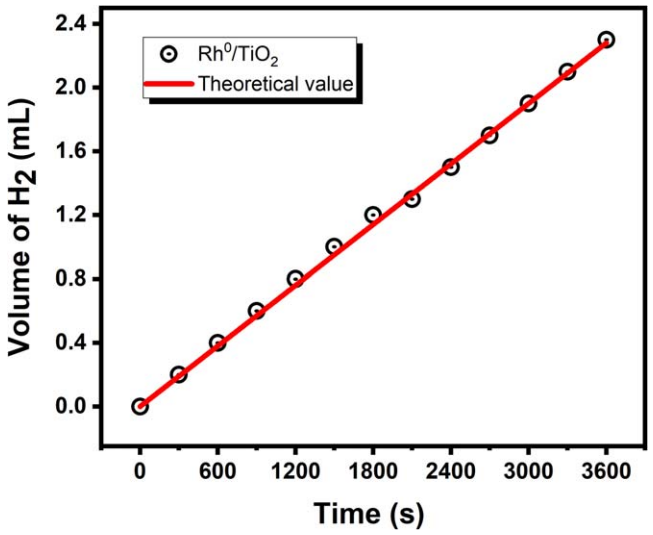

Figure 7. The amount of generated H_2 (ml) vs time graph during the electrolysis of H_2O using Rh^0/TiO_2 in 0.5 M H_2SO_4. (See SI for the theoretical yield calculation).

frequency regions in Fig. 6a can be fitted to the model depicted in the inset figure. Note that CPE_2 and R_2 can be attributed to the left semicircles at high frequency region in this model. These semicircles are potential independent and arise from the contact between the catalyst surface and the GCE (porosity or adsorbed species on GCEs). The other semicircle at low frequency region is potential dependent and its radius decreases with increasing potential, indicating a faster charge transfer at higher overpotentials. CPE_1 and R_1 belonging to this semicircle refer to double layer capacitance (C_{dl}) and charge transfer resistance (R_{ct}), respectively. R_s in the model is uncompensated solution resistance and used for the iR correction. The Tafel slope can also be calculated by using EIS results. This calculation method is only related to the charge transfer kinetics and allows us to exclude contribution coming from the catalyst resistance.[59] From the η vs log ($1/R_{ct}$) plot, the Tafel slope value was calculated as 33 mV dec^{-1} which is quite similar to the one derived from the LSV curve. Moreover, the electrochemical surface area, ECSA, of Rh/TiO_2-2000 was determined as 15.35 cm^2 by dividing (C_{DL} was found as 6.14 * 10^{-4} F from impedance curve at onset potential) to specific capacitance of flat electrode (Cs ~40 μF cm^{-2}).[60]

The HER activity of Rh^0/TiO_2-2000 was also calculated from chronopotentiometry. A constant current of 5.0 mA (corresponding to η = 100 mV) was applied for the 3600 s at ~25 °C in 0.5 M H_2SO_4. The volume of the evolved H_2 gas from the water electrolysis was measured in a Hoffman electrolysis cell and followed as a function of time (Fig. 7). The Faradaic efficiency of Rh^0/TiO_2-2000 for HER was calculated as 94% after applying the charge of 18000 mC (see SI for the related calculations). The calculated yield is consistent with the theoretical one and also comparable to that of the reported catalysts. For example, the Faradic yield was found as 86%, 95% and 100% for Mn_2O_3-SC-TT,[33] Ru1-GC[61] and Rh_2P@NC,[19] respectively.

Conclusions

In this study, rhodium nanoparticles on TiO_2 were successfully prepared by following a facile impregnation-reduction method. The electrocatalytic activity of Rh^0/TiO_2-2000 on GCE with an ultralow mass loading of rhodium (3.79 μg cm^{-2}) in hydrogen evolution reaction was investigated in acidic media. Rh^0/TiO_2-2000 provides very low Tafel slope (32 mV dec^{-1}), low overpotential (37 mV@ −10 mA cm^{-2}), high exchange current density (0.686 mA cm^{-2}), and high TOF value (11.45 s^{-1}). The Faradaic efficiency of Rh^0/TiO_2-2000 was found as 94% after applying 18000 mC. The Tafel slope and overpotential @ −10 mA cm^{-2} values are found to be nearly the same with the one obtained by using the benchmark Pt/C catalyst. Rh^0/TiO_2-2000 on GCE provides high stability even after 10000 cycles in HER. There is no noticeable change in the onset potential (29 mV), overpotential (40 mV@ −10 mA cm^{-2}), and Tafel slope (33.1 mV dec^{-1}) after the stability test. The high durability and high efficiency of Rh^0/TiO_2-2000 make it a promising electrocatalyst for hydrogen evolution reaction.

ORCID

Ahmet M. Önal https://orcid.org/0000-0003-0644-7180

References

1. W.-F. Chen, J. T. Muckerman, and E. Fujita, *Chem. Commun.*, **49**, 8896 (2013).
2. N. S. Lewis and D. G. Nocera, *Proc. Natl Acad. Sci.*, **103**, 15729 (2006).
3. A. Demirbaş, *Energy Sources*, **27**, 741 (2005).
4. M. Balat and M. Balat, *International Int. J. Hydrogen Energy*, **34**, 3589 (2009).
5. F. Cheng and V. Dupont, *Catalysts*, **7**, 114 (2017).
6. A. Haryanto, S. Fernando, N. Murali, and S. Adhikari, *Energy Fuels*, **19**, 2098 (2005).
7. B. Eliasson, C. Liu, and U. Kogelschatz, *Ind. Eng. Chem. Res.*, **39**, 1221 (2000).
8. Z. Pu, Y. Luo, A. M. Asiri, and X. Sun, *ACS Appl. Mater. Interfaces*, **8**, 4718 (2016).
9. J. D. Benck, T. R. Hellstern, J. Kibsgaard, P. Chakthranont, and T. F. Jaramillo, *ACS Catal.*, **4**, 3957 (2014).
10. Q. Gu, Z. Gao, S. Yu, and C. Xue, *Adv. Mater. Interfaces*, **3**, 1500631 (2016).
11. A. J. Arvia, A. E. Bolzán, and M. Á. Pasquale, *Catalysis in Electrochemistry*, ed. E. Santos and W. Schmickler (John Wiley & Sons, Inc., United States of America)17 (2011).
12. J. R. McKone, E. L. Warren, M. J. Bierman, S. W. Boettcher, B. S. Brunschwig, N. S. Lewis, and H. B. Gray, *Energy Environ. Sci.*, **4**, 3573 (2011).
13. J. Greeley, T. F. Jaramillo, J. Bonde, I. Chorkendorff, and J. K. Nørskov, *Nature Mater.*, **5**, 909 (2006).
14. M. Hu, M. Ming, C. Xu, Y. Wang, Y. Zhang, D. Gao, J. Bi, and G. Fan, *ChemSusChem*, **11**, 3253 (2018).
15. L. Zhang, L. Liu, H. Wang, H. Shen, Q. Cheng, C. Yan, and S. Park, *Nanomaterials*, **7**, 103 (2017).
16. L. Zhu, H. Lin, Y. Li, F. Liao, Y. Lifshitz, M. Sheng, S.-T. Lee, and M. Shao, *Nat. Commun.*, **7**, 12272 (2016).
17. B. Jiang, L. Yang, F. Liao, M. Sheng, H. Zhao, H. Lin, and M. Shao, *Nano Res.*, **10**, 1749 (2017).
18. J. Du, X. Wang, C. Li, X.-Y. Liu, L. Gu, and H.-P. Liang, *Electrochim. Acta*, **282**, 853 (2018).
19. Z. Pu, I. S. Amiinu, D. He, M. Wang, G. Li, and S. Mu, *Nanoscale*, **10**, 12407 (2018).
20. M. Zeng and Y. Li, *J. Mater. Chem. A*, **3**, 14942 (2015).
21. W. Wang, T. He, X. Liu, W. He, H. Cong, Y. Shen, L. Yan, X. Zhang, J. Zhang, and X. Zhou, *ACS Appl. Mater. Interfaces*, **8**, 20839 (2016).
22. M. Liu, R. Zhang, and W. Chen, *Chem. Rev.*, **114**, 5117 (2014).
23. F. Song, W. Li, and Y. Sun, *Inorganics*, **5**, 40 (2017).
24. E. Demir, S. Akbayrak, A. M. Önal, and S. Özkar, *J. Colloid Interface Sci.*, **531**, 570 (2018).
25. M. Akbayrak and A. M. Önal, *J. Electrochem. Soc.*, **166**, H897 (2019).
26. C. Xu, M. Ming, Q. Wang, C. Yang, G. Fan, Y. Wang, D. Gao, J. Bi, and Y. Zhang, *J. Mater. Chem. A*, **6**, 14380 (2018).
27. S. G. Kumar and K. S. R. K. Rao, *Nanoscale*, **6**, 11574 (2014).
28. S. Akbayrak, S. Gençtürk, İ. Morkan, and S. Özkar, *RSC Adv.*, **4**, 13742 (2014).
29. X. Zheng, L. Li, M. Deng, J. Li, W. Ding, Y. Nie, and Z. Wei, *Catal. Sci. Technol.*, **10**, 4743 (2020).
30. S.-Y. Huang, P. Ganesan, S. Park, and B. N. Popov, *J. Am. Chem. Soc.*, **131**, 13898 (2009).
31. J. Park, S. Lee, H.-E. Kim, A. Cho, S. Kim, Y. Ye, J. W. Han, H. Lee, J. H. Jang, and J. Lee, *Angew. Chem. Int. Ed.*, **58**, 16038 (2019).
32. D. Panayotov, E. Ivanova, M. Mihaylov, K. Chakarova, T. Spassov, and K. Hadjiivanov, *Phys. Chem. Chem. Phys.*, **17**, 20563 (2015).
33. S. Hernández, C. Ottone, S. Varetti, M. Fontana, D. Pugliese, G. Saracco, B. Bonelli, and M. Armandi, *Materials*, **9**, 296 (2016).
34. G. Wang, S. Jing, and Y. Tan, *Sci. Rep.*, **7**, 16465 (2017).
35. Y. Okamoto, N. Ishida, T. Imanaka, and S. Teranishi, *J. Catal.*, **58**, 82 (1979).
36. L. Li, G. Zhang, B. Wang, T. Yang, and S. Yang, *J. Mater. Chem. A*, **8**, 2090 (2020).
37. S. Cherevko, A. R. Zeradjanin, G. P. Keeley, and K. J. J. Mayrhofer, *J. Electrochem. Soc.*, **161**, H822 (2014).
38. C. Zhang, Y. Hong, R. Dai, X. Lin, L.-S. Long, C. Wang, and W. Lin, *ACS Appl. Mater. Interfaces*, **7**, 11648 (2015).
39. N. Lotfi, T. Shahrabi, Y. Yaghoubinezhad, and G. B. Darband, *Appl. Surf. Sci.*, **505**, 144571 (2020).
40. S. Alayoglu and B. Eichhorn, *J. Am. Chem. Soc.*, **130**, 17479 (2008).
41. A. Fan, C. Qin, X. Zhang, J. Yang, J. Ge, S. Wang, X. Yuan, S. Wang, and X. Dai, *J. Mater. Chem. A*, **7**, 24347 (2019).
42. H. Duan et al., *J. Am. Chem. Soc.*, **139**, 5494 (2017).
43. J. Scremin et al., *Nanoscale Adv.*, **12**, 18214 (2020).

44. J. Gao, X. Tang, P. Du, H. Li, Q. Yuan, G. Xie, and H.-J. Qiu, *Sustain. Energy Fuels*, **4**, 2551 (2020).
45. F. Yang, Y. Zhao, Y. Du, Y. Chen, G. Cheng, S. Chen, and W. Luo, *Adv. Energy Mater.*, **8**, 1703489 (2018).
46. J. Yu, D. Wei, Z. Zheng, W. Yu, H. Shen, Y. Qu, S. Wen, Y.-U. Kwon, and Y. Zhao, *J. Colloid Interface Sci.*, **566**, 505 (2020).
47. B. T. Jebaslinhepzybai, N. Prabu, and M. Sasidharan, *Int. J. Hydrogen Energy*, **45**, 11127 (2020).
48. K. M. Naik, E. Higuchi, and H. Inoue, *Nanoscale*, **12**, 11055 (2020).
49. X. Meng, C. Ma, L. Jiang, R. Si, X. Meng, Y. Tu, L. Yu, X. Bao, and D. Deng, *Angew. Chem. Int. Ed.*, **59**, 10502 (2020).
50. K. Eiler, S. Suriñach, J. Sort, and E. Pellicer, *Appl. Catal., B.: Environ.*, **265**, 118597 (2020).
51. D. Yoon, B. Seo, J. Lee, K. S. Nam, B. Kim, S. Park, H. Baik, S. Hoon Joo, and K. Lee, *Energy Environ. Sci.*, **9**, 850 (2016).
52. T. Kim, J. Park, H. Jin, A. Oh, H. Baik, S. H. Joo, and K. Lee, *Nanoscale*, **10**, 9845 (2018).
53. N.-A. Nguyen, V.-T. Nguyen, S. Shin, and H.-S. Choi, *J. Alloys Compd.*, **789**, 163 (2019).
54. D. Bhalothia, S.-P. Wang, S. Lin, C. Yan, K.-W. Wang, and P.-C. Chen, *Applied Sciences*, **10**, 5155 (2020).
55. M. D. Sharma, C. Mahala, and M. Basu, *J. Colloid Interface Sci.*, **534**, 131 (2019).
56. B. Jiang, Y. Sun, F. Liao, W. Shen, H. Lin, H. Wang, and M. Shao, *J. Mater. Chem., A*, **5**, 1623 (2017).
57. M. Smiljanić, I. Srejić, B. Grgur, Z. Rakočević, and S. Štrbac, *Electrochem. Commun.*, **28**, 37 (2013).
58. J. Li, X. Zhou, Z. Xia, Z. Zhang, J. Li, Y. Ma, and Y. Qu, *J. Mater. Chem. A*, **3**, 13066 (2015).
59. H. Vrubel, T. Moehl, M. Grätzel, and X. Hu, *Chem. Commun.*, **49**, 8985 (2013).
60. X. Zhao, X. He, F. Yin, B. Chen, G. Li, and H. Yin, *Int. J. Hydrogen Energy*, **43**, 22243 (2018).
61. J. Creus, S. Drouet, S. Suriñach, P. Lecante, V. Collière, R. Poteau, K. Philippot, J. García-Antón, and X. Sala, *ACS Catal.*, **8**, 11094 (2018).